Pharmacological Research - Modern Chinese Medicine 3 (2022) 100074

Contents lists available at ScienceDirect

Pharmacological Research - Modern Chinese Medicine

journal homepage: www.elsevier.com/locate/prmcm

Sesquiterpene Lactones Modulated DNA Methylation through Inhibition of DNMTs in Ovarian Cancer Cells

Idowu Fadayomi[a], Suat Sari[b], Mark Kitchen[a], Jóhannes Reynisson[a], Nicholas Forsyth[a], Wen-Wu Li[a,*]

[a] School of Pharmacy and Bioengineering, Keele University, Stoke-on-Trent, ST4 7QB, UK
[b] Department of Pharmaceutical Chemistry, Faculty of Pharmacy, Hacettepe University, 06100, Ankara, Turkey

ARTICLE INFO

Keywords:
Ovarian cancer
Sesquiterpene lactone
Dehydroleucodine
DNA methylation
DNMT inhibitors
Apoptosis

ABSTRACT

Inappropriate DNA methylation of tumour suppressor genes can affect their expression and function, and as such, DNA methylation has been a promising target for anti-cancer therapy. In gynaecological malignancy, ovarian cancer has the highest associated rate of mortality. This study investigated the *in vitro* cytotoxicity of four sesquiterpene lactones (SLs), including dehydroleucodine (Deh), alantolactone (Ala), costunolide (Cos), and parthenolide (Pat), and their effect on DNA methylation in ovarian cancer. The binding of the SLs with DNA methyltransferases (DNMTs) were studied using molecular docking. The *in vitro* antiproliferative activity was evaluated in human ovarian cancer cell lines. SL-induced pro-apoptotic activity and effect on cell cycles was evaluated using enzymatic assays and flow cytometry. Global DNA methylation and DNMTs activity by SLs were measured using ELISA assays. DNA methylation and expression of tumour suppressor genes *MHL1* and *PTEN* were quantified using pyrosequencing and RT-qPCR, respectively. SLs displayed strong binding to DNMT1, 3A and 3B in silico, with Deh exhibiting the strongest binding. SLs showed cytotoxicity in the order of Deh ≈ Ala > Pat > Cos, induced apoptosis, and arrested cell cycle at G2/M phase. Deh and Ala possessed DNMT inhibitory activity, reduced global and gene-specific DNA methylation, and increased expression of notable *MHL1* and *PTEN*, which could contribute to the induction of apoptosis and cell death. In conclusion, Deh and Ala, possess strong cytotoxicity and hold the exciting potential as novel therapeutic agents in ovarian cancer.

Introduction

DNA methylation is among the underlying mechanisms for multi-step processes driving the transformation of normal cells into tumour cells. Aberrant DNA methylation of CpG rich regions, known as CpG islands (CGI), especially at the gene promoter region (approximately 70% of mammalian genes have promoter associated CGIs) [1], is known to contribute to the regulation of gene expression. Where such abnormal methylation is associated with recognised or putative tumour suppressor genes or oncogenes, altered expression may impact various cellular mechanisms and cell cycle control, causing or contributing ultimately to cancer formation [2,3]. As a key mechanism of gene expression regulation, DNA methylation is maintained throughout the genome and during cell division, by the DNA methyltransferases (DNMTs). Inappropriate methylation of tumor suppressor genes (typically hypermethylation of promoter-associated CGIs), can result in their transcriptional silencing and lead to tumor development; thus, inhibition of inappropriate DNA methylation changes in cancer cells, can be effective in 'normalizing' cellular processes such as differentiation and apoptosis [4]. There are three active types of DNMTs, namely DNMT1, DNMT3a and DNMT3b, the last two of which share a high level of homology. Structurally the enzymes consist of a catalytic and DNA recognition domain at the *C* terminal, and a regulatory domain at the *N* terminal. Methyltransferase functionality is mediated by the co-factor, *S*-adenosyl-L-methionine (SAM), which transfers a methyl group to the cytosine of CpG, and is simultaneously converted to the co-factor product *S*-adenosyl-L-homocysteine (SAH) [2,5]. Another type, DNMT3L, although catalytically inactive alone, is associated with DNMT3a and DNMT3b, and also participates in transcriptional regulation [6]. Two DNMT inhibitors 5-azacytidine (Aza) and decitabine have been approved for clinical use in the treatment of chronic myelomonocytic leukaemia, and acute myeloid leukaemia [7,8].

Ovarian cancer is the eighth most common malignancy worldwide, and the seventh highest in terms of cancer mortality rate [9]. The treatment for ovarian cancer is multimodal, and may include

Abbreviations: Ala, alantolactone; 5Aza, 5-azacytidine; Cos, costunolide; CGI, CpG islands; Deh, dehydroleucodine; DNMTs, DNA methyltransferases; Pat, parthenolide; SLs, sesquiterpene lactones; SRB, sulforhodamine B.

* Correspondence author.
E-mail address: w.li@keele.ac.uk (W.-W. Li).

https://doi.org/10.1016/j.prmcm.2022.100074
Received 10 February 2022; Received in revised form 27 February 2022; Accepted 1 March 2022
Available online 2 March 2022

surgery, chemotherapy, radiotherapy, and/or immunotherapy [10]. The chemotherapeutic drug are mainly paclitaxel, carboplatin, and inhibitors of poly(ADP-ribose) polymerase (PARPi). Each of these options can have significant patient side-effects, and may be limited by availability, cost, lack of efficacy, and development of drug resistance. Therefore, the search for novel therapies is vitally important to overcome the current clinical difficulties and improve quantity and quality of life for women with ovarian cancer [11].

There are two major DNA methylation pattern changes in ovarian cancer, and indeed in many other tumour types, site-specific and promoter-associated CGI hypermethylation, and gene-body hypomethylation. Inappropriate methylation patterns can affect the transcriptional competence of a variety of genes, importantly, including tumour suppressor genes such as *BRCA1* and *P53*. Abnormal transcription and function of such genes is vital for normal cellular processes such as DNA repair, cell cycle progression, cell adhesion, apoptosis and angiogenesis. Loss of regulation in any of these functions or processes may lead to cancer development. Furthermore, inappropriate gene body and repeat sequence hypomethylation can result in genomic instability and chromosomal rearrangement, and loss of transcriptional silencing of oncogenes, again promoting tumour development [12,13]. Many tumour suppressor genes transcriptionally silenced by DNA hypermethylation have been well characterized in multiple tumour types, these include: *PTEN, TP53, HOXA9*, and *hMLH1* [14–16]. Mutations of these genes using CRISPR-Cas9 genome editing techniques in mouse cells generated ovarian tumour, proving their importance in ovarian cancer [17]. The promoter region of *KF14*, an oncogene that codes for a mitotic kinase, has been shown to be hypomethylation and over-expressed in ovarian cancer [18]. The increased expression of this gene, thought secondary to methylation change, could therefore be an important therapeutic target [19]. Additionally, hypermethylation of the promoter regions of the tumour suppressor genes including Tumour Suppressor Candidate 3 (*TUSC3*) [20] and Deleted in Lung and Esophageal Cancer 1 (*DLEC1*) [21], has also been associated with reduced expression of these genes in epithelial ovarian cancer. Therefore, drug-mediated epigenetic modulation (of DNA methylation) could be an important target for novel treatment in ovarian cancer, namely by resetting DNA methylation to re-induce the 'normal' transcriptional silencing of oncogenes and/or increasing the expression of repressed tumour suppressor genes [19].

Plant-derived natural products (e.g. paclitaxel) or extracts have been used or investigated for ovarian cancer treatment [22]. Furthermore, small molecules [23] including both synthetic [24] and natural products [25] have been explored for their effect on DNA methylation for cancer treatment. Phytochemicals such as curcumin, epigallocatechin-3-gallate, genistein [25], S-allycysteine[26], and ginsenoside Rg3 [27] have all been shown to inhibit DNMT activity and alter DNA methylation patterns. Many of these compounds are widely present in traditional Chinese medicine [28]. Sesquiterpene lactones (SLs) are a large group of natural products comprising of 15-carbon atoms with three isoprene units and a lactone group. The cytotoxicity of SLs to cancer cells was first found fifty years ago [29]. Since then, many SLs have been discovered and demonstrated to have the ability to target specific signalling pathways, making them good candidates for drug discovery [30] and repurposing in various tumour types [31]. Currently, SLs or their derivatives such as artesunate, dimethylaminoparthenolide, and a thapsigargin derivative are being evaluated in the cancer clinical trials [32,33]. SLs in various traditional Chinese medicine showed a plethora of biological activities including anticancer potential. For example, dehydroleucodine (Deh) isolated in the Chinese medicinal plant *Artemisia atrovirens* [34] and *A. douglasiana* [35] showed gastroduodenal mucosal protection [36], inhibition of chemicals-induced mast cell degranulation [37] and neuropeptide-induced mast cell activation [38]. Deh also showed cytotoxicity in mouse melanoma cells and a mouse melanoma model [39], human astrocytoma [40] and leukaemia cells [41]. Alantolactone (Ala) present in traditional Chinese medicine *Inula helen*ium L [42]. exhibited cytotoxicity in lung [43,44], glioblastoma [45] and breast [46] cancer cells. Parthenolide (Pat) from *Tanacetum parthenium* showed anti-thyroid cancer activity [47]. Costunolide (Cos) present in the Chinese medicine such as *Aucklandia lappa* Decne [48] and *Saussurea lappa* Clarks inhibited autophagy in hepatocellular carcinoma cells [49]. Despite the potential relevance of these compounds in cancer treatment, little is known about their roles in epigenetic regulation, especially in DNA methylation and inhibition of DNMTs, although a previous study has shown that Pat inhibited DNMT1 [50]. Here we sought to explore the potential cytotoxicity of the four selected SLs (Deh, Ala, Cos, and Pat) [51], and further evaluated their roles in DNMT inhibition, DNA methylation, and impact upon patterns of gene expression in ovarian cancer cells.

Materials and Methods

Deh, Ala, 4', 6-diamidino-2-phenylindole (DAPI), copper (II) sulphate solution, propidium iodide, and Ribonuclease A from bovine pancreas were from Sigma Aldrich. Pat, Cos, and Aza were purchased from Abcam Plc, UK (Table S1). Caspase-Glo 3/7, caspase-Glo 8 and caspase-Glo 9 assay kits, and high-performance GoTaq® G2 DNA polymerase with Mg-free buffer system were from Promega, UK. Trichloroacetic acid (TCA), mitoprobe DiIC1 assay kit, actinRed™ 555 ReadyProbes™ reagents, TAE buffer (Tris-acetate-EDTA) (50x), gene ruler 100 bp plus DNA ladder and dNTP mix were products of Fisher scientific, UK.

RNase A, RNeasy Mini Kit, DNeasy Blood and Tissue Kit and QuantiFast SYBR® Green RT-PCR Kit were from Qiagen, UK. Ethidium bromide, agarose, PyroMark PCR kit, PyroMark gold Q24 reagents, PyroMark wash buffer, PyroMark binding buffer, PyroMark annealing buffer, streptavidin sepharose™ high performance and primers were also from Qiagen (Table S1). MethylFlash Global DNA Methylation (5-mC) ELISA Easy Kit (Colorimetric), EpiQuik DNMT Activity/Inhibition Assay Ultra Kit (Colorimetric), EpiQuik Nuclear Extraction Kit, and EZ DNA Methylation Kit Gold were from Epigentek. Annexin V-FITC, annexin V buffer and propidium iodide solution were from Miltenyi Biotec Ltd.

Molecular modelling

The ligand models were generated and optimized using MacroModel (2019-2, Schrödinger, LLC, New York, NY, 2019) according to the OPLS_2005 force field parameters and conjugate gradient method [52]. The molecular descriptors were calculated using QikProp (2019-2, Schrödinger, LLC, New York, NY). For human DNMT1 (Protein data bank (PDB) ID: 4WXX, resolution: 2.62 Å) [5], for human DNMT3A crystal structures (PDB ID: 5YX2, resolution: 2.65 Å) [53] were downloaded from the RCSB Protein Data Bank (www.rcsb.org), while the human DNMT3B structure was built by homology modelling on MODELLER [54] using DNMT3A crystal structure as template [55]. For homology modelling of DNMT3B, the query and template sequences were aligned pairwise, and 100 initial models were built according to this alignment. The co-crystallized ligand in the template's catalytic site, SAH, as well as the water molecules, was transferred from the template to the models. The best model was selected upon discrete optimized protein energy (DOPE) scores. The protein structures were prepared for docking using Protein Preparation Wizard of Maestro (2019–2: Schrödinger, LLC, NY, 2019) [56] of Maestro (2019–2: Schrödinger, LLC, NY, 2019). During this process, unwanted residues were removed, missing side chains were filled, hydrogens were added, bond orders were assigned, ionization and tautomeric states were generated, and proton orientations were set (Epik 2019–2: Schrödinger, LLC, NY, 2019; Prime 2019–2: Schrödinger, LLC, New York, 2019). DNMT3B homology model was further subjected to restrained minimization with converging heavy atoms to a root-mean square deviation (RMSD) value of 0.30 Å for heavy atoms, and then analyzed using PROCHECK server [57]. For molecular docking Glide (2019-2: Schrödinger, LLC, NY, 2019) [58–60], AutoDock (v4.2, The Scripps Research Institute, San Diego, CA) [61] and AutoDock Vina (v1.1.2, The Scripps Research Institute, San Diego, CA) [62] were used. Grid maps

of the receptor active sites large enough to accommodate the ligands were prepared using the receptor grid generation panel of Maestro for Glide and AutoGrid for AutoDock. The centroid coordinates of the co-crystallized ligand (DNMT1: -47.39 61.24 7.04; DNMT3A: 60.52 32.41 -21.22; DNMT3B: 60.50 32.39 -21.25) were taken as the center of search space for each protein and the grid size was set as 27,000 $Å^3$. For Glide, standard precision mode was used; for AutoDock, Lamarckian genetic algorithm was selected, and the docking simulations were run 50 times per ligand. For AutoDock Vina, the default settings were preserved. Following visual evaluation, the docking score of the best pose of each ligand was noted.

Cell culture

The human ovarian cancer cell lines (CIS-A2780, OVCAR-8 and OVCAR-4) were products of the American type culture collection (ATCC). CIS-A2780 cell line is a derivate of the A2780 cells previously exposed to cisplatin which made the cells cisplatin-resistant. The normal human ovarian epithelial (HOE) cells were purchased from Applied Biological Materials (ABM) Inc.

The Rosewell Park Memorial Institute (RPMI 1640, Lonza) medium with 10% foetal bovine serum (FBS), 2 mM glutamine and 50 μg/mL penicillin-streptomycin (Pen strep) were used to culture the cancer cells and HOE cells [63,64]. Cells were grown and maintained in a standard humidified incubator at 37°C, in 5% carbon dioxide (CO_2) conditions throughout this study.

Cell growth inhibitory assay

The cytotoxicity of the four SLs and positive control Aza were investigated using sulforhodamine B (SRB) assay as described previously [63,64]. The data were analysed by non-linear regression using the Graph pad PRISM 6.0 software to fit a 4 parameter sigmoidal dose-response curve to determine IC_{50} values. Three independent and three replicates of experiments were performed.

Trypan blue assay

The cytotoxicity of the four SLs and cell viability was studied using trypan blue assay (TBA) [64]. Briefly, the cells (CIS-A2780, OVCAR-8, and OVCAR-4) were seeded in 12 well plates at a density of 1×10^5 cells per well in 1mL of growth media. Three different concentrations of the studied compounds (5, 10 and 20 μM) were administered to the cells after 24 h incubation. Medium containing 0.1% DMSO was used as negative control, while Aza was used as positive control. Cell viability was determined using haemocytometer and trypan blue exclusion at different time points (24, 48 and 72 h) after treatment. The percentage (%) of cell death was thereafter determined and data presented in graph.

Apoptosis detection using caspase 3/7, 8 and 9 markers

Caspase 3/7, 8 and 9 activities was analysed using caspase-Glo 3/7, 8 and 9 assay kits on 96-well microplates according to the manufacturer's instruction and as previously reported [64,65]. Briefly, the cells (CIS-A2780, OVCAR-8 and OVCAR-4) were seeded in 96 well plates at a cell density of 5000 cells/well in 80 μL growth media, and exposed to two different doses (10 and 20 μM) of each compound after 24 h incubation. After 48 h exposure to the treatment compounds, 25 μL of Caspase 3/7, 8 and 9 Glo-reagents were added, and the cells incubated further in the dark for 40 min on a gentle rocker. The luminescence was measured with microplate reader at 570nm. SRB assay was performed for each treatment at the same condition on different well plates, to help quantify the actual caspase 3/7 activation with response to compound treatment and cell number.

Flow cytometry analysis of cell apoptosis

Annexin V-FITC and propidium iodide staining of CIS-A2780 cell line were carried out using flow cytometry as described previously [64]. Briefly, cells were seeded in 12 well plates at a density of 2×10^5 cells per well in 1 mL of growth media and incubated for 24 hours. Two different concentrations of the studied compounds (IC_{50} value and 2x IC_{50} value of each compound) were administered to the cells after 24 hours incubation with 0.1% of DMSO in medium included as negative control. Supernatant was aspirated and cells were re-suspended in 500 μL binding buffer before 5 μL of propidium iodide was added to distinguish cells in early apoptosis from cells in late apoptosis, prior to flow cytometry analysis on Beckman Coulter Cytoflex equipped with CytExpert software for data acquisition and analysis. Prior to cell analysis on flow cytometry, daily QC was performed to verify the alignment of the cytoflex flow cytometer. The population of the cell was gated on the side scatter area (SSC) and forward scatter area (FSC) to exclude the debris and doublet. The data was distributed in the FITC and PE channels. The data was analyzed using the CytExpert software.

Cell cycle analysis

The effect of the four SLs on the cell cycle in CIS-A2780 cell line was studied using flow cytometry as previously described [64]. Cells were seeded in 12 well plates at a density of 2×10^5 cells per well in 1 mL of growth media and incubated for 24 hours. Two different concentrations of the studied compounds at approximate (IC_{50} value and x 2 of IC_{50} value of each compound) were administered to the cells after incubation for 24 hours. 0.1% of DMSO in medium was used as negative control. In all cell cycle assays, cell pellets were collected after 48 hours of treatment with each compound to evaluate their early effects on cell homeostasis. The cell cycle phase was presented using histogram on the PE channel with count on the vertical channel using the CytExpert software.

Evaluation of inhibitory activity of SLs against DNMT

Nuclear extraction of CIS-A2780 cells was performed using the Epiquick™ nuclear extraction kit. The inhibition of DNMT activity by the SLs at two different concentrations was carried out using the EpiquickTM DNMT activity/inhibition assay ultra-kit (colorimetric assay) according to the manufacture protocol (Supporting information).

Quantification of global and gene specific DNA methylation

CIS-A2780 cells were seeded in 6 well plates at a density of 4×10^5per well in 2 mL of growth media, and incubated for 24 hours. Two different concentrations of the studied compounds at IC_{50} value and 2x of IC_{50} value were administered to the cells, after 72 hours of incubation cells were harvested. 0.1% medium was used as negative control. DNA was extracted using QIAamp DNA mini kit (Qiagen) according to the manufacturer's instructions. The total 5-methylcytosine content in DNA was detected using MethylFlash™ Global DNA methylation (5-mC) ELISA easy kit (Colorimetric) (Epigentek NY, USA) according to the manufacturer's instructions (detail see Supporting Information).

Pyrosequencing assay for quantification of gene promoter specific DNA methylation

PyroMark assay design 2.0 software used to design primers (forward, reverse, and sequencing primers with either the forward or reverse primer biotin labelled) (Table S2). *MLH1* and *PTEN* were evaluated. DNA was extracted from CIS-A2780 cells and bisulfite converted. Bisulfite conversion was performed with EZ DNA methylation-Gold™ kit from Zymo research (Epigenetics Company) according to the manufacturer's instruction (Supporting information). PCR was performed

Table 1
The chemical structure, calculated descriptors and number of RO5 violations of the four SLs and Aza.

Comp.	RB (0-15)	MW (130 – 725 Da)	HD (0-6)	HA (2-20)	LogP (-2.0-6.5)	PSA (7-200 Å^2)	RO5
Deh	1	244.3	0	5	1.5	66.3	0
Ala	1	232.3	0	3	2.8	38.2	0
Cos	1	232.3	0	3	2.7	40.6	0
Pat	1	248.3	0	5	1.8	46.1	0
Aza	5	244.2	5	11.8	-2.6	153.8	0

using PyroMark® PCR kit from Qiagen. Bisulfite converted DNA was used as starting material. The PCR product was checked by agarose gel analysis prior to pyrosequencing. PyroMark Q24 reagents and system were used for analysis of pyrosequencing reactions. The pyroMark Q24 machine protocol for pyrosequencing and Qiagen protocol were used in this study (Supporting Information). The percentage methylation at each CpG site was identified for further analysis.

Quantitative reverse transcription polymerase chain reaction (RT-qPCR)

RNA was extracted from CIS A270 cells using RNeasy Min kit. RT-qPCR was performed using QuantiFast® SYBR green RT-PCR kit. Primers were designed using the Integrated DNA technologies PrimerQuest® Tool, the gene transcripts were determined and obtained from Ensembl/National Center for Biotechnology Information (NCBI) (Table S3). Primer-BLAST was done to check for primer specificity, and primer self-complementarity check was also done and melting temperatures (Tm) were determined. All the primers used were desalted and optimised to determine their optimum annealing temperatures. The PCR plates were placed in the real-time cycler and the thermal cycling programme was run (Supplementary materials). The Ct values were arranged in excel worksheet and the mRNA expression was determined with the Ct values, the relative gene expression changes were calculated based on 2 (-Delta Delta Ct) method [66]. *GAPDH* was used as an internal control gene to normalize the variations in gene expression.

Statistical analysis

All data generated from this study were organized in Microsoft Excel and were independently subjected to statistical analyses for better interpretation and presentation using GraphPad prism 6 software (GraphPhad Software Inc.). One-way analysis of variance (ANOVA) and student t test were used to evaluate potential differences between the mean of control and treatments and mean of treatment at different concentrations were significant. Post hoc Dunnetts' test was used to determine which of the concentration of the treatment was significant to the control, while the Tukey test was used to determine which of the concentration of a particular treatment was significant when compared. The significance level at $p < 0.05$, $p < 0.01$, $p < 0.001$ and $p < 0.0001$ are represented as (*), (**), (***) and (****).

Results

Evaluation of the chemical space of the four selected SLs

Plant-derived SLs were evaluated in terms of drug-likeness using the molecular descriptors [67] which define drug-like chemical space (molecular weight MW, number of rotatable bonds RB, H bond donor count HD, H bond acceptor count HA, logarithm of octanol/water partition coefficient LogP, and polar surface area PSA) (Table 1). Compounds were also checked for violations of the Lipinski's rule of five (RO5) (HD ≤ 5, HA ≤ 10, MW < 500, LogP ≤ 5), an accepted criteria set for orally active drugs [68].

Table 1 presents an ideal values range that defines the drug-like chemical space limits for each descriptor. The descriptors are within these ranges for the compounds except Aza, which had very low LogP value. All the compounds complied with the RO5 showing that the compounds have the potential for development as drug candidates.

Molecular modelling

Currently available 3D structures of human DNMT3B do not cover the catalytic site. Therefore we created a homology model of human DNMT3B with the catalytic domain and substrate using comparative modelling approach [69]. According to the Basic Local Alignment Search Tool (BLAST), DNMT3A crystal structure showed the highest sequence homology to DNMT3B. Among these structures, 5YX2 was selected due to its resolution and percentile ranks. Using this structure as template and a pairwise sequence alignment, initial 100 DNMT3B models were built. The model with the lowest DOPE score (-33107.26 kcal/mol) was selected and analyzed regarding stereochemical quality by PROCHECK. According to the Ramachandran plot, 94.3% of the amino acids were in the core region and only one (Asn626) was in the disallowed region (Fig. S1). The model satisfied all the side chain parameters, and all the planar groups were within their accepted limits.

Molecular docking

The crystallographic data available for DNMT1, 3A and 3B so far suggest a number of potential ligand binding sites including co-factor binding site and the catalytic site, however there is only one human X ray DNMT1 structure with an inhibitor, sinefungin (adenosyl-ornithine) (PDB ID: 3SWR). Sinefungin is a natural analogue of SAH with antifungal, antiviral and antiparasitic activity through RNA and DNA methyltransferase inhibition (Fig. S2) [70,71]. Sinefungin is observed to bind to the co-factor site in a very similar way as SAH and SAM. For this reason, we explored the binding interactions of the ligands in the co-factor binding site of the selected crystal structures and homology model, all of which include SAH to enable comparison of the docking results. First, we re-docked SAH to the target proteins and calculated the root-mean-square deviation (RMSD) values regarding its original conformer in each protein. On Glide the RMSD values were 1.14, 0.61, and 0.33 Å; on AutoDock 2.36, 0.51, and 0.88 Å; on AutoDock Vina 1.00, 0.51, and 1.40 Å for DNMT1, DNMT3A and DNMT3B, respectively. These results indicate reliability for these methods with the preferred settings and protein structures.

Docking scores, or fitness scores, predicted by the molecular docking software suits provide estimations of the strength of a given ligand-receptor complex. For the docking scores from the software used in this study, lower values indicate higher affinity. According to Table 2 it can be suggested the overall affinity of the compounds were slightly higher for DNMT1 than to DNMT3A, which also provides an understanding of the selectivity level for the compounds toward the three DNMTs although the selectivity in the scoring functions may not be observed *in vitro*. According to Glide, Aza has the best scores in the series with especially higher affinity to DNMT3B than the other compounds. Also, Deh has good scores, especially with DNMT1. According to AutoDock and AutoDock Vina Deh is the top–scoring compound.

The compounds with better scores were observed to interact with the important residues for forming complexes with SAH (Fig. S3). Deh forms an H-bond with Cys1191 of DNMT1 according to Glide and with Gly1149 and Leu1151 according to AutoDock, which are one of the key

Table 2
Docking scores of the binding of four SLs and Aza to three DNMTs using Glide, AD and AD Vina (kcal/mol).

	DNMT1			DNMT3A			DNMT3B		
Comp.	Glide	AD	AD Vina	Glide	AD	AD Vina	Glide	AD	AD Vina
Deh	-6.7	-7.9	-7.1	-5.5	-7.8	-7.5	-4.7	-7.6	-6.8
Ala	-5.7	-6.2	-6.8	-5.1	-6.8	-5.9	-3.8	-6.3	-5.9
Cos	-5.2	-6.9	-7.0	-6.0	-6.8	-5.9	-4.6	-6.4	-6.3
Pat	-4.9	-6.3	-6.8	-4.4	-5.1	-4.1	-3.4	-5.2	-4.5
Aza	-6.6	-2.9	-6.9	-6.5	-2.4	-7.0	-6.0	-2.8	-7.3

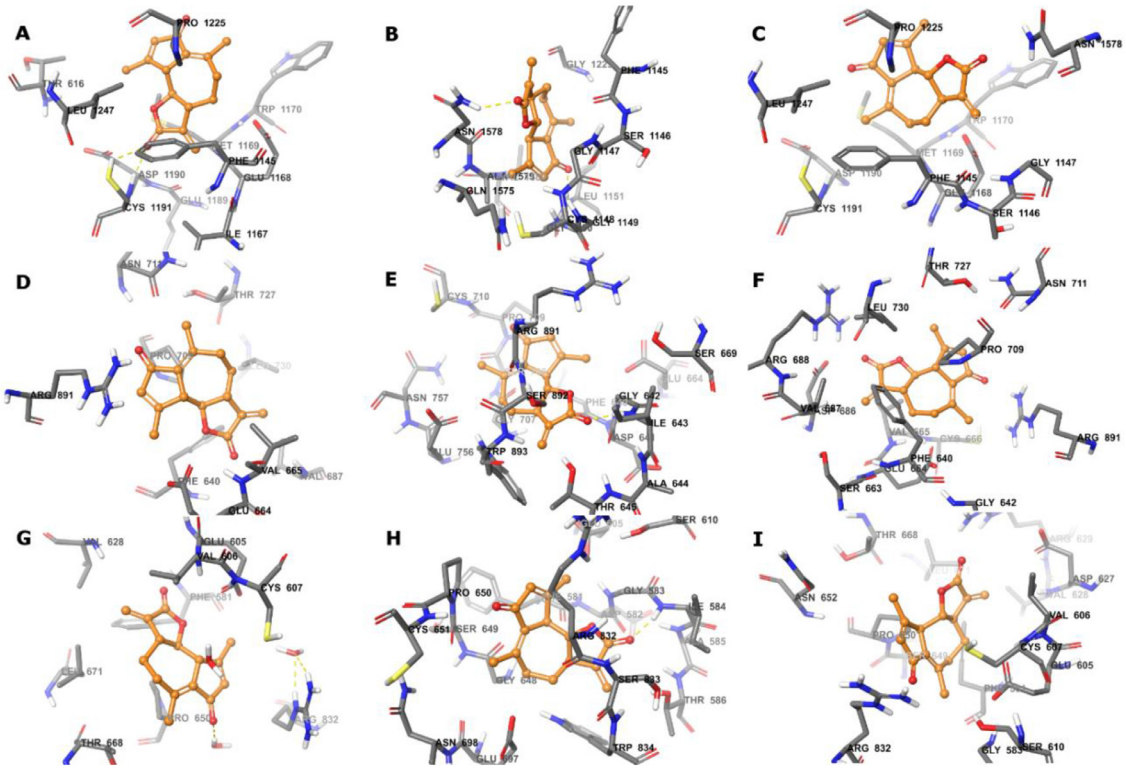

Fig. 1. Binding interactions of Deh with the co-factor binding site residues of DNMT1 (A-C), DNMT3A (D-F), and DNMT3B (G-I) predicted by Glide (A, D, G), AutoDock (B, E, H), and AutoDock Vina (C, F. I), respectively. Ligands are represented as stick-and-balls, residues as sticks, and H-bond interactions as yellow dashed lines.

residues of the SAH-DNMT1 complex (Fig. 1). AutoDock also predicts an H-bond between Deh and Ile643 of DNMT3A, as well as between Deh and Ile584 of DNMT3B, which are also highlighted in SAH-DNMT3A and SAH DNMT3B complexes, respectively. The tetrahydrofuranone moiety of Deh is responsible for these interactions.

Antiproliferative activity of sesquiterpene lactones (SLs)

The antiproliferative activity of the four SLs and 5-azacytidine (Aza) were evaluated by the growth of three ovarian cancer cell lines (CIS-A2780, OVCAR-8 and OVCAR-4) and immortalised normal human ovarian epithelial (HOE) cells (Fig. 2). The selectivity indexes (SIs) against CIS-A2780 cell line were determined. The four SLs significantly inhibited ovarian cancer growth with IC_{50} values of 2.0-12.2μM. Deh, and Ala showed higher *in vitro* anti-ovarian cancer activity with the lower IC_{50} values than Pat and Cos with their slightly higher IC_{50} values (Fig. 2A and B). The positive control (Aza) displayed a significant growth inhibitory activity with IC_{50} values of 3.5-6.4 μM. Furthermore, the growth inhibitory activity of the four SLs was higher against CIS-A2780 and OVCAR-8 than OVCAR-4 cells (Fig. 2B). In addition, the higher IC_{50} values of each of the SLs on HOE, compared with ovarian cancer cell lines, indicated that SLs possess stronger antiproliferative activity against ovarian cancer cell lines than HOE cells. All SLs showed SI around 3-4.3, while Aza less than 1. The SI results suggest that the antiproliferative activity of Cos and Pat are more cancer specific than Deh and Ala, while Aza showed the least cancer specific activity.

We next confirmed that the cytotoxicity of these SLs was caused via induction of cell death in three cell lines with three different concentrations (5, 10 and 20 μM) at 24h, 48h, and 72 h (Fig. 2C, Fig. S4).

Induction of apoptosis by SLs

Light and fluorescence microscopy were used in the evaluation of change in the morphology of cellular, nuclear and actin structures of ovarian cancer cell lines after treatment with SLs. Changes in cellular structure (Fig. S5) and disruption to the actin filament networks (Fig. S6) are clearly observed, which indicate induction of apoptosis.

Caspase 3/7, 8 and 9 activities were next evaluated following SLs and Aza treatment of three ovarian cancer cell lines. The four SLs increased the activity of caspase 3/7 in CIS-A2780 cells (Fig. 3A). Deh, Ala and Pat showed similar caspase 3/7 activity in CIS-A2780 cells with 11-, 1-2 and 15-fold increase respectively, while Cos caused the lowest increase in caspase 3/7 activity, with 5-fold increase at the highest concentra-

A)

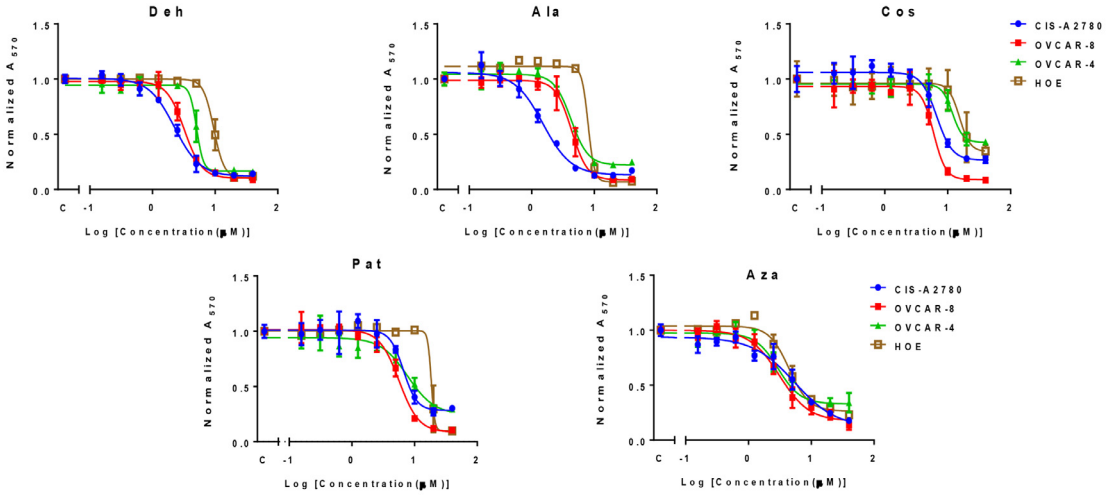

B)

Compounds	IC_{50} ± SEM (μM)				SI against CIS-A2780
	CIS-A2780	OVCAR-8	OVCAR-4	HOE	
Deh	2.4±0.2	4.1±1.5	7.4±1.9	8.7±0.4	3.6
Ala	2.0±0.4	4.6±0.5	7.4±0.8	8.2±0.4	4.1
Cos	8.1±1.4	7.8±1.9	12.2±0.7	25.2±0.3	3.1
Pat	5.7±0.5	7.2±2.4	10.7±2.0	24.3±3.9	4.3
Aza	6.4±0.8	3.5±0.4	3.8±0.3	4.9±0.6	0.8

C)

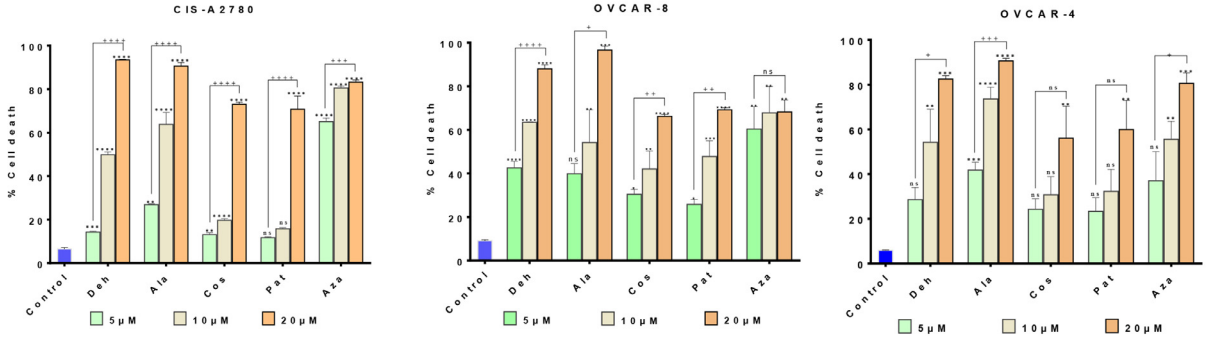

Fig. 2. SLs induce cytotoxicity in ovarian cancer cells. A, Mean concentration-response curves of antiproliferative activities of SLs and Aza on CIS-A2780, OVCAR-8, OVCAR-4 and HOE cell lines using cell growth inhibitory SRB assay. All cell lines were treated with different concentrations of each compound (0.16-40 μM) for 72h. The data generated were analysed as mean ± SEM of five repeated experiments. The negative control is denoted with C (cells without drug dose i.e. only medium with 0.2% DMSO). B, The IC_{50} results were generated from concentration-response curves, which are expressed as mean ± SEM of five independently repeated experiments in triplicate. SI is the ratio of IC_{50} of HOE to IC_{50} on CIS-A2780 cell line. C, Trypan blue exclusion cytotoxic assay at different concentrations (5, 10 and 20 μM) after 72 hours treatment of SLs. Aza was used as positive control and negative control group was treated with ordinary medium with 0.1% DMSO. The percentage cell deaths were estimated and recorded as means ± SEM of three repeated experiments. The significant level of the Dunnett's multiple comparison test of each compound with the control is denoted with asterisk (*), while the concentration dependent activity significant level using one-way ANOVA is represented as plus (+). The significance level at $p < 0.05$, $p < 0.01$, $p < 0.001$ and $p < 0.0001$ are represented as (*), (**), (***) and (****). Similar pattern was followed for significant difference within concentrations of the same compound.

tion. The positive control (Aza) showed the highest caspase 3/7 activity with 28-fold increase over the negative control. All of the SLs induced concentration-dependent changes in caspase 3/7 activities. Similar patterns of increased caspase 3/7 activity were observed in OVCAR-8 and OVCAR-4 cell lines (Fig. 3A).

Caspase 8 activity of the positive control (Aza) was 13-fold higher than negative control, and significantly higher than the caspase 8 activity of each of the SLs in CIS-A2780 cells (Fig. 3B). Ala showed 5-fold higher caspase 8 activity, while Deh, Pat and Cos showed an approximately 2-fold increase in caspase 8 activity. However, in OVCAR-8 and OVCAR-4 cells, there was a significant increase of caspase 8 activity for all four SL, in a concentration-dependent manner (Fig. 3B).

Caspase 9 activity in CIS-A2780 cells significantly increased after treatment with the four SLs and the positive control (Aza), when compared with the negative control, with Ala showing the highest (10-fold) increase, while Deh and Pat showed a 3-fold increase, and Cos showed a 2-fold increase at higher concentration (Fig. 3C). Aza stimulated a 22-fold higher increase of caspase 9. Similarly, the four SLs and Aza further increased caspase 9 activities in OVCAR-8, with only Deh, Ala and Cos showing significant effect on caspase 9 activity at both concentrations (10 and 20 μM). The increase in caspase 9 activity found after Pat and Aza treatment was only significant at higher concentration (20 μM). Ala, Cos and Pat stimulated a 5-, 4- and 4-fold caspase 9 increase, respectively, while Deh and Aza led to only a 3-fold increases. In OVCAR-4

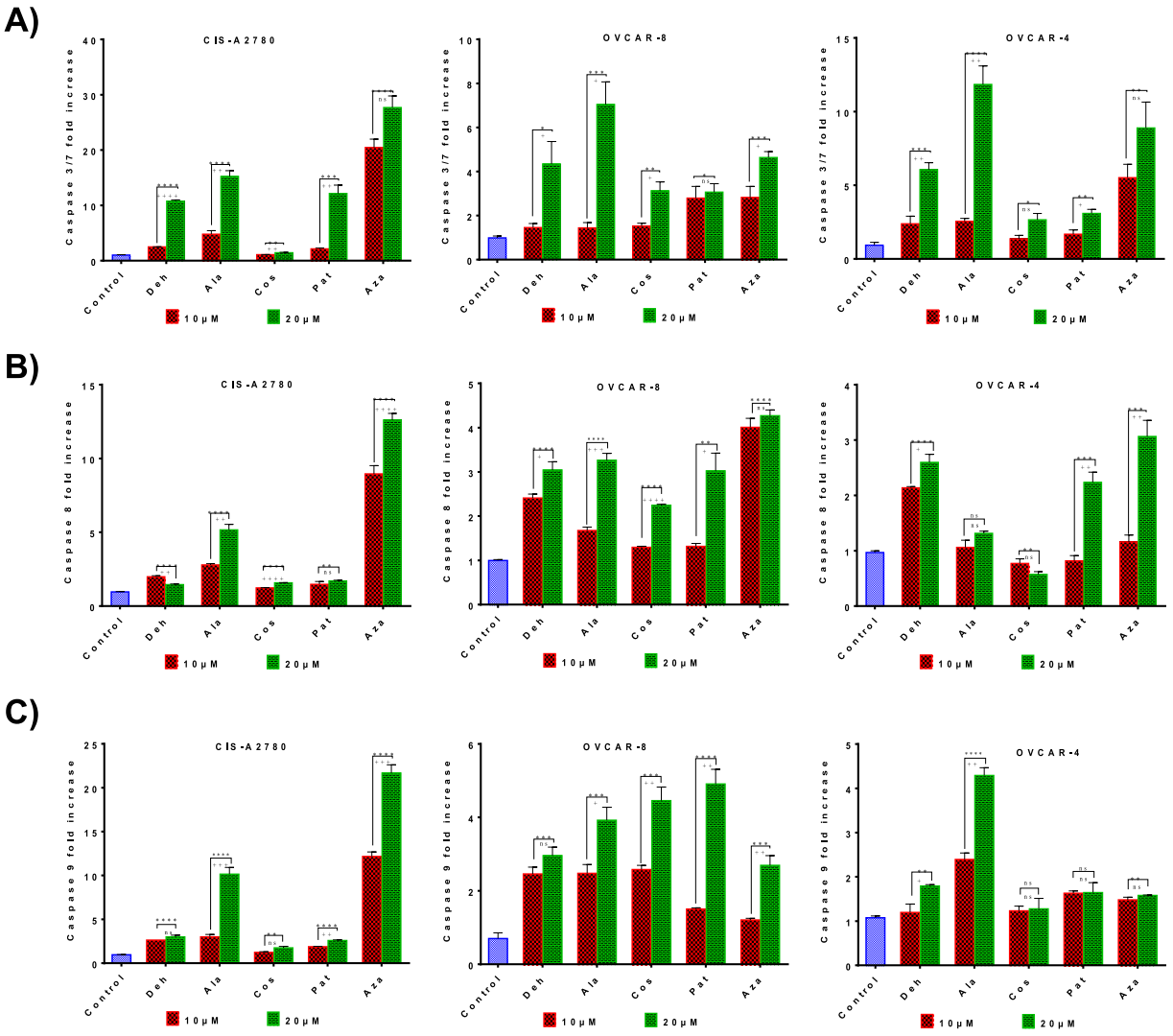

Fig. 3. Effect of SLs on caspase activity. A, Caspase 3/7 activity in ovarian cancer CIS-A2780, OVCAR-8 and OVCAR-4 cell lines; B, Caspase 8 activity; C, caspase 9 activity. Aza (at the same concentrations as the four SLs) and 0.2% DMSO were used as positive and negative controls, respectively. The fold increase in caspase 3/7, 8 and 9 activities of each compound was compared with the negative control (0.2% DMSO) using one-way ANOVA with Dunnett's multiple comparisons test, and student t test was used to test caspase concentration dependent activity. Significance difference between SLs and control is denoted with asterisk (*) (*, $p < 0.05$, **, $p < 0.01$, ***, $p < 0.001$ and ****, $p < 0.0001$), while significant concentration dependent activity was denoted with plus (+) in a similar manner.

cells, Deh, Ala and Aza were the only compounds that significantly increased caspase 9 activity, with Ala causing the highest caspase activity (4-fold increase), while Cos and Pat did not significantly increase caspase 9 activity in OVCAR-4 cell line (Fig. 3C). The caspase 9 activity by Deh in OVCAR-4 was comparable to Aza.

To further elucidate the mechanism of action of these SLs causing cytotoxicity to cancer cells, Cis-A2780 cell line was used as a model for in depth investigation. Evaluation of the pro-apoptotic activity of SLs and Aza was first assessed using annexin V and propidium iodide (PI) staining. The four SLs and Aza induced significant apoptosis when compared with the control (Fig. 4). The percentage of early and late apoptosis induced by Ala at 5 μM (25.4% and 36.7%) and 10 μM (8.3% and 64.1%) respectively, were higher than that of Deh at 5 μM (14.2% and 10.9%) and 10 μM (16.3% and 27.5%), Pat at 10 μM (11.0% and 10.4%) and 20 μM (26.6% and 30.0%) and Cos at 10 μM (13.7% and 9.0%) and 20 μM (21.4% and 49.4%) respectively. Furthermore, the percentage of apoptosis induced by Ala and Cos was relative to that of the positive control (Aza) at 5μM (13.8% and 63.3%) and 10 μM (13.1% and 68.7%) respectively. Only Cos and Pat showed concentration dependent apoptotic activity in CIS-A2780.

Cell cycle analysis of ovarian cancer cell lines in response to SLs treatment

The four SLs and the positive control Aza significantly reduced the percentage of cells at the G_0-G_1 phase when compared with control. Additionally, Ala, Cos and Aza reduced the percentage of cells in the G_0-G_1 phase at both lower and higher concentrations, while Deh and Pat only reduced it at higher concentrations (Fig. 5). The four SLs arrested cells at both S and G_2-M phase, while Aza caused profound cell-cycle arrest at S phase. Ala, Cos, Pat and Aza increased the percentage of cells in the sub-G_1 phase, consistent with the apoptosis assay findings. Deh with strong pro-apoptotic activity only slightly increased sub-G_1 population.

DNMT inhibitory activities of SLs and Aza

Ala, Pat and Aza significantly inhibited the enzymatic activity of DNMTs in CIS-A2780 cell line (Fig. 6A), while a slight inhibitory activity was also found in Deh-treated cells. However, all four SLs and Aza showed more significant inhibition of DNMTs in OVCAR-4 cells with Cos the lowest (Fig. 6B).

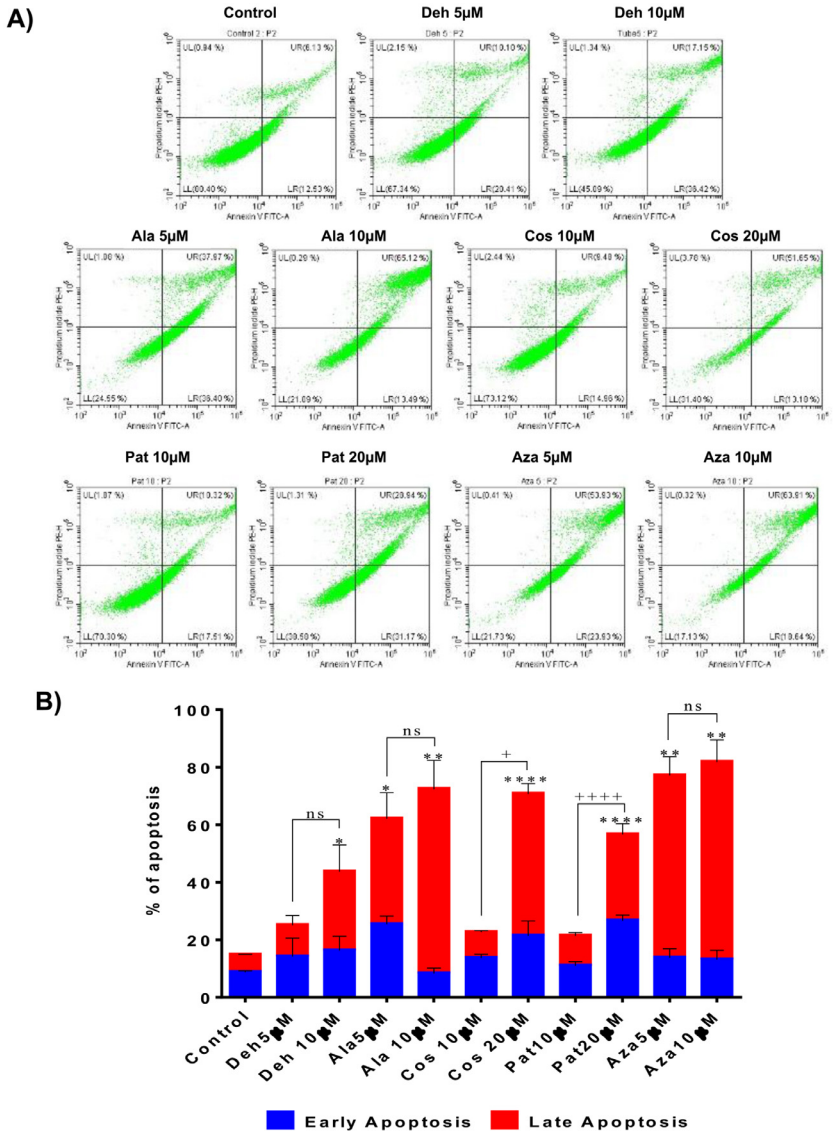

Fig. 4. Flow cytometry analysis of the apoptotic activities of SLs and Aza using annexin V and propidium iodide staining. A) Flow cytometry graph of CIS-A2780 cell line treated with four SLs and Aza. Lower left (LL), upper left (UL), lower right (LR) and upper right (UR) represent live cells, necrotic cells, cells in early apoptosis and cells in late apoptosis respectively. B, Analysis of the apoptotic activities. The data represent the mean ± SD of three repeated experiments. The apoptotic activity of each compound was compared with the control using one-way ANOVA with Dunnett's multiple comparisons test denoted with asterisk (*) and student t test was used to test for concentration dependent activity denoted with plus (+). (*, $p < 0.05$, **, $p < 0.01$, ***, $p < 0.001$ and ****, $p < 0.0001$).

Effect of DNA methylation by four SLs

The four SLs and Aza significantly reduced the level of global DNA methylation compared with the negative control (Fig. 7A). Change in the methylation profiles of promoters of two tumour suppressor genes, mutL homolog 1 (*MLH1*), and phosphatase and tensin homolog (*PTEN*), were evaluated. Deh and Ala reduced CpG methylation at the promoters of *MLH1* and/or *PTEN* compared to the untreated control (Fig. 7B and 7C). However, Cos, Pat and Aza did not show significant changes relative to control.

Effect of SLs on tumour suppressor gene expression by RT-qPCR

qPCR was performed to assess the effects of the SLs and Aza on the expression of *MLH1* and *PTEN*. Ala treatment caused about 10-fold increase of expression of *MLH1* while others did not (Fig. 8A). Deh and Ala increased around 15 and 40-fold expression of *PTEN,* respectively, while Cos, Pat and Aza also increased but with less extent (Fig. 8B).

Discussion

The in vitro anti-ovarian cancer activities of four selected SLs were investigated in this study with a focus on their potential impact upon DNA methylation and induction of apoptosis. Initial molecular modelling of the four SLs with the DNMTs suggested high affinity to DNMT1, DNMT3A, and DNMT3B, showing somewhat higher selectivity for DNMT1. Aza has been demonstrated to resemble cytidine which is then incorporated into DNA where it covalently traps DNMTs to DNA, leading to DNA damage and cell death [8]. Our molecular docking shows non-covalent binding of Aza to the DNMTs providing possible and addtional mechanism for its action. The docking scores were generally in accordance with inhibitory activity of DNMTs, and decrease of global and some gene specific DNA methylation in promoter regions.

Pat observations were consistent with a previous study that demonstrated Pat decreased global DNA methylation in breast cancer [50]. Pat also decreased gene-specific promoter methylation of *HIN-1* in breast cancer. Similarly, Aza treatment also decreased global DNA methylation. Comparable global and gene-specific promoter DNA demethylating activity of Aza has also been reported in different cancer types such as lymphoid, myeloid, and colorectal cancer [72,73]. Each of the SLs investigated, Ala, Deh, Pat and Aza demonstrated significant DNMT enzymatic inhibitory activity. Concerning the tumour suppressor genes investigated, Deh decreased the promoter associated CGI methylation of both *MLH1* and *PTEN*, it did not appear to affect its expression of *MHL1* but significantly increased the expression of *PTEN* (Fig. 8). Ala decreased the CpG methylation of promotors of both *MLH1 and PTEN,* it also signif-

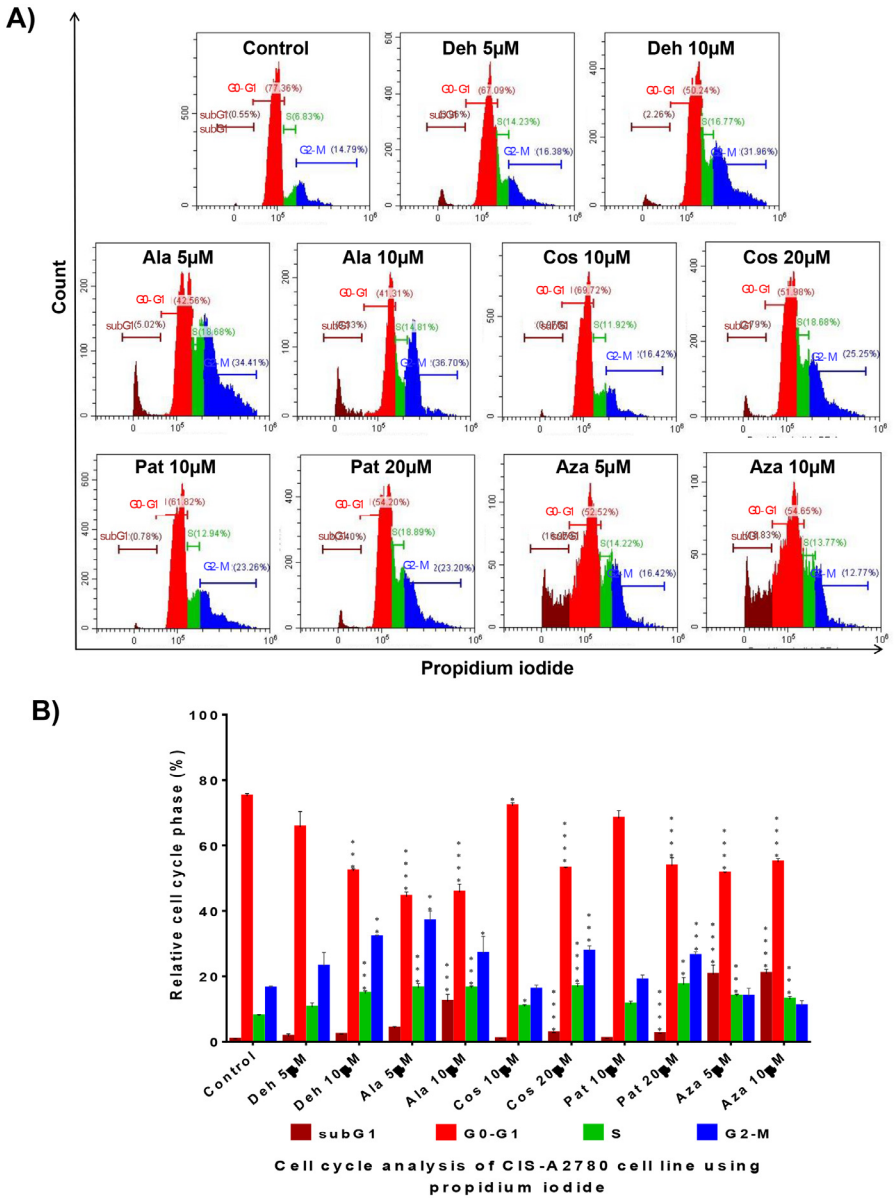

Fig. 5. Flow cytometry analysis of the cell cycle activity of SLs and Aza on CIS-A2780 cell line using propidium iodide staining. A) Flow cytometric graphs of cells after treatment. B) Analysis of the cell populations at different cell cycle phase. These data represent the mean ± SD of three repeated experiments. The cell-cycle effects of each compound at the three individual phases were compared with the control using one-way ANOVA with Dunnett's multiple comparisons test; the significance level is denoted with asterisk (*). (*, $p < 0.05$, **, $p < 0.01$, ***, $p < 0.001$ and ****, $p < 0.0001$).

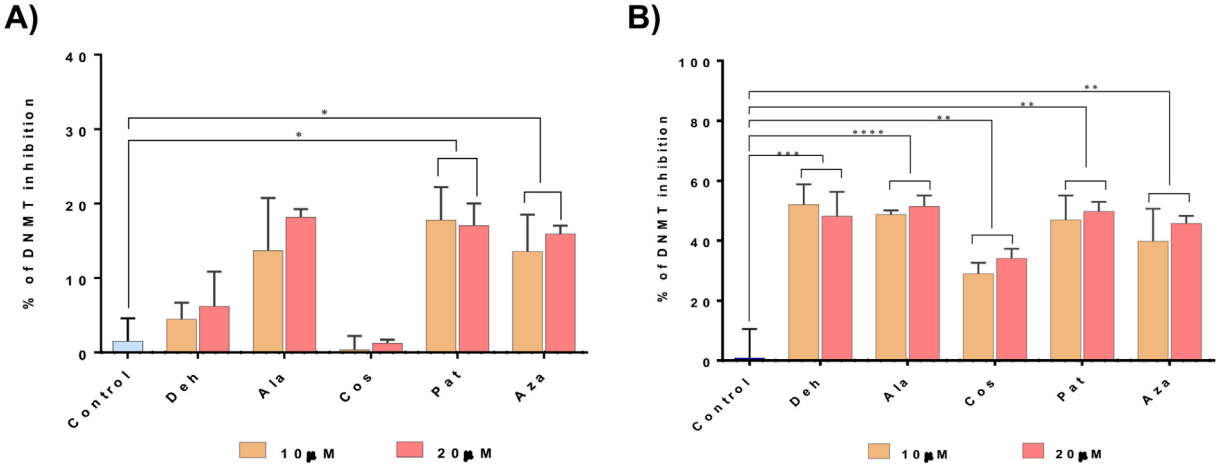

Fig. 6. DNMT-inhibitory activities of the SLs and Aza A) Percentage of inhibition of DNMTs in CIS-A2780 cells. B) Percentage of inhibition of DNMTs in OVCAR-4 cells. Aza was used as positive control. Data are presented as mean ± SD (n=3). The DNMT inhibitory activity of each SL was compared with the control using one-way ANOVA, and the significant level is denoted with asterisk (*). p value < 0.05 (*), < 0.01 (**), < 0.001 (***) and <0.0001 (****).

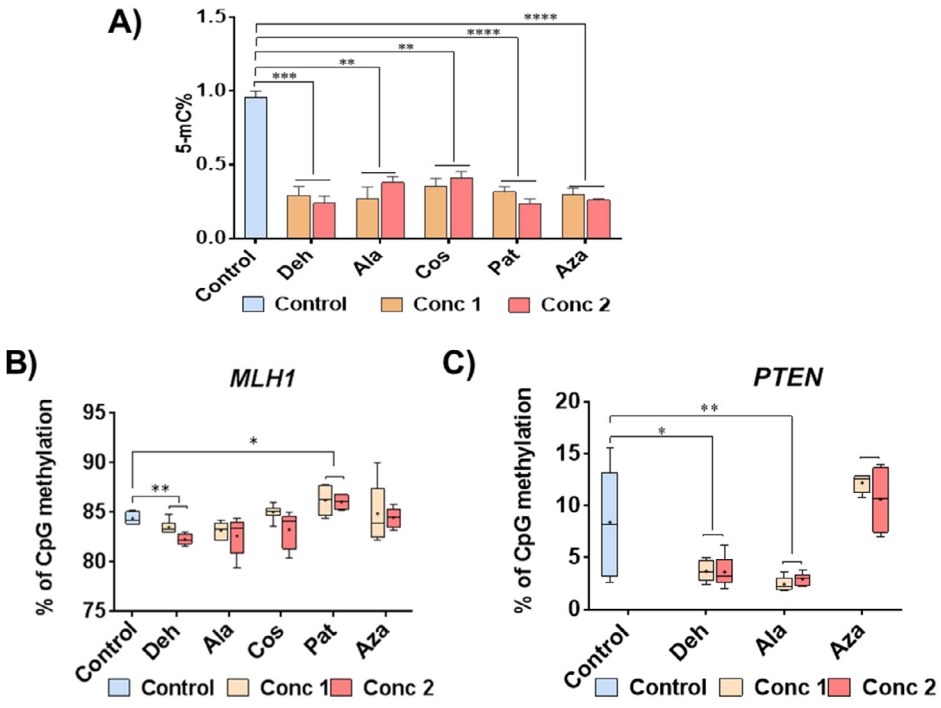

Fig. 7. Effect of SLs on DNA methylation in ovarian cancer cells. A) Global DNA methylation change in CIS-A2780 cells after treatment of the four SLs. The percentage of 5-mC was presented as 5mC/(5mC + C). B) The percentage of gene-specific promoter associated CpG island methylation of *MLH1*, and C) The percentage of CpG island methylation of the promoter of *PTEN* genes in ovarian cancer cell line (Cis-A2780) in response to SLs treatment, using Aza as positive control. Conc. 1 and 2 are 5 and 10 μM for Deh, Ala and Aza, respectively, and 10 and 20 μM for Pat and Cos. Results are presented as mean ± SD of three repeats in duplicate. Significant differences between each compound activity compared with the control, using one-way ANOVA, are denoted with asterisk (*). P value < 0.05 (*) and < 0.01 (**)

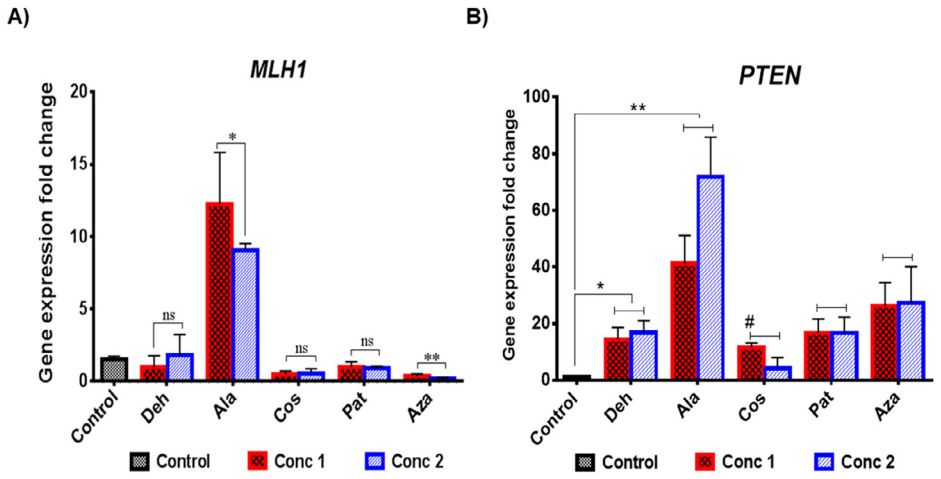

Fig. 8. Changes in tumour suppressor gene expression following treatment with the four SLs and Aza. RT-qPCR results of two tumour suppressor genes *MLH1* (A) and *PTEN* (B) were presented as mean ± SD of three repeats. Data were analysed using one-way ANOVA to test for significant differences in the expression level of each gene in the control and treated samples.

icantly increased the expression of both genes. These significant effects are likely due to the inhibition of DNMTs mainly DNMT1 by these SLs consistent with the modelling results that Deh and Ala have the strongest binding affinities with DNMTs. However, Cos and Pat did not show much change of the methylation of promoter of *MLH1*, with also no significant change of its expression. They caused slight increase of expression of *PTEN* but not significantly comparing to control, however their effect on their methylation level was not further determined. Aza decreased global level of DNA methylation, but had less effect on these two specific gene promotors. There is strong correlation between promoter hypermethylation of *PTEN* gene and activation of DNMT1[74]. In ovarian cancer, *PTEN* gene negatively regulates the PI3K/AKT/mTOR signalling pathway involved in several important cell functions such as cell proliferation and survival [16]. Therefore, the high antiproliferative and apoptotic activities of Deh and Ala are suggested to be mediated by their DNMTs inhibitory activity and gene expression modulatory capacity.

The four SLs tested had a high growth inhibitory activity in ovarian cancer cell lines with IC_{50} between 2.0-12.2 μM. They inhibited the growth of CIS-A2780 and OVCAR-8 cells with lower IC_{50} values, but inhibited OVCAR-4 cells with slightly higher IC_{50} values, suggestive of cell line dependent activity. Deh and Ala inhibited the growth of ovarian cancer cell lines at lower IC_{50} values compared with higher IC_{50} values of Cos and Pat. The growth inhibitory activity of Deh on ovarian cancer cell lines reported in this study was similar to those previously described in acute myeloid leukaemia [41] and breast cancer [75]. Furthermore, the cytotoxic activities of the four SLs were potentially cancer-specific, with reduced cytotoxicity against immortalised HOE cells with lower expression of *DNMT1* and *DNMT3b* [76], thus suggesting the inhibition of these DNMTs by SLs. Pat and Cos were shown to be less cytotoxic to HOE than Deh and Ala. Although S-allycysteine from gallic [26], and ginsenoside Rg3 from *Panax* species [27] were demonstrated to be DNMT inhibitors and activate expression of tumour suppressor genes in ovarian cancer cells, much higher concentrations are needed to achieve such effect. The four SLs present in different Chinese medicine have shown greater potency against ovarian cancer and this study has enriched our understanding of the mechanisms of action of traditional Chinese medicine in the treatment of cancer via epigenetic modulation[28].

The cytotoxicity of each of the four SLs was investigated further to establish their roles in the induction of cell death through apoptosis.

SLs induced significant apoptosis in ovarian cancer cells. The apoptotic activity of the SLs was concentration dependent. Ala showed the highest apoptotic activity. The four SLs and Aza induced apoptosis through the activation of caspase 3/7, which is an apoptosis executioner marker. Furthermore, the mechanism of apoptosis induction activities of SLs and Aza was by both extrinsic and intrinsic pathways through caspase dependent activity which was shown via activation of caspase 8 (marker of extrinsic pathway) and 9 (marker of intrinsic pathway) activities. Deh and Ala induced apoptosis in lung [43,44], and breast cancer cells [39], respectively. Similarly, Ala, Cos and Aza reduced the activity of the mitochondrial membrane potentials likely causing the release of cytochrome *c* into the cytoplasm and activating the cascade of caspase 9 through an intrinsic pathway. Ala has also increased the expression of caspase 3 and 9 in glioblastoma, and further induced the release of cytochrome *c* into the cytoplasm [45]. Furthermore, Ala has been found to induce apoptosis in breast cancer cell lines and caused cell cycle arrest at G_2-M phase [46].

In addition to the apoptotic activity of SLs, they caused cell cycle arrest in the ovarian cancer cell line. Deh and Aza caused cell cycle arrest at G_2-M phase, while Ala, Pat and Cos arrested the cells at S and G_2-M phases, and subsequently resulted in a significant decrease in the number of cells in the G_0-G_1 phase, and increase in the percentage of cells in the subG_1 phase. The cell cycle arrest induced by these compounds was similar to previous reports showing that Deh induced cell cycle arrest at G_2-M phase in human cerebral astrocytoma [40] and breast cancer. Likewise, Ala can induce cell cycle arrest at G_2-M phase in liver cancer [77].

There are several limitations in the current study First, the epigenetic mechanism of SLs was only investigated in the cisplatin resistant CIS-A2780 cell line, which could be extended to its parent cisplatin sensitive A2780 and normal HOE cells to see if these SLs play roles in the development and drug resistance in ovarian cancer. Second, only two tumour suppressor genes and the change of methylation level of their promotors were studied. Additional genes with higher methylation levels could be further investigated. Third, we still do not know which of DNMTs is responsible for the binding of SLs and how strong the binding is, so the experimental and direct inhibition of individual DNMT by SLs should be carried out to fully understand their mechanisms of action.

Conclusion

In summary, the *in silico* molecular modelling of the four SLs with DNMTs along with experimental studies on their mechanisms of action in ovarian cancer cells was investigated. Deh and Ala showed DNMT inhibitory, DNA demethylating activities, consequent increase in tumour suppressor gene expression leading to induction of apoptosis and cell death. Deh and Ala are potential candidates for novel ovarian cancer treatment. Our study is the first to report the DNMT inhibitory and DNA hypomethylation activities of Deh and Ala in ovarian cancer cells. However, further investigation of their efficacy, side-effect profile and tolerability *in vivo* is needed before we can consider these viable drug treatment options in women with ovarian cancer.

Declaration of Competing Interest

The authors declare no potential conflicts of interest.

Acknowledgement

We thank Dr. Joseph Kwong for reading the manuscript and Dr. Alan Richardson's support.

Funding

Nigerian Tertiary Education Trust Fund (TETFUND) for a PhD fellowship to Idowu Fadayomi.

Supplementary materials

Supplementary material associated with this article can be found, in the online version, at doi:10.1016/j.prmcm.2022.100074.

References

[1] M.A. Dawson, T. Kouzarides, Cancer epigenetics: from mechanism to therapy, Cell 150 (1) (2012) 12–27.
[2] K.D. Robertson, DNA methylation and human disease, Nat Rev Genet 6 (8) (2005) 597–610.
[3] P.A. Jones, J.P. Issa, S. Baylin, Targeting the cancer epigenome for therapy, Nat Rev Genet 17 (10) (2016) 630–641.
[4] C.B. Yoo, P.A. Jones, Epigenetic therapy of cancer: past, present and future, Nat Rev Drug Discov 5 (1) (2006) 37–50.
[5] Z.M. Zhang, S. Liu, K. Lin, Y. Luo, J.J. Perry, Y. Wang, J. Song, Crystal Structure of Human DNA Methyltransferase, J Mol Biol 427 (15) (2015) 2520–2531.
[6] F. Chedin, The DNMT3 family of mammalian de novo DNA methyltransferases, Prog Mol Biol Transl Sci 101 (2011) 255–285.
[7] E.J. Derissen, J.H. Beijnen, J.H. Schellens, Concise drug review: azacitidine and decitabine, Oncologist 18 (5) (2013) 619–624.
[8] K. Agrawal, V. Das, P. Vyas, M. Hajduch, Nucleosidic DNA demethylating epigenetic drugs - A comprehensive review from discovery to clinic, Pharmacol Ther 188 (2018) 45–79.
[9] L.A. Torre, B. Trabert, C.E. DeSantis, K.D. Miller, G. Samimi, C.D. Runowicz, M.M. Gaudet, A. Jemal, R.L. Siegel, Ovarian cancer statistics, 2018, CA Cancer J Clin 68 (4) (2018) 284–296.
[10] L. Kuroki, S.R. Guntupalli, Treatment of epithelial ovarian cancer, BMJ 371 (2020) m3773.
[11] M. McMullen, K. Karakasis, R. Rottapel, A.M. Oza, Advances in ovarian cancer, from biology to treatment, Nat Cancer 2 (1) (2021) 6–8.
[12] S. Sharma, T.K. Kelly, P.A. Jones, Epigenetics in cancer, Carcinogenesis 31 (1) (2010) 27–36.
[13] M.A. Earp, J.M. Cunningham, DNA methylation changes in epithelial ovarian cancer histotypes, Genomics 106 (6) (2015) 311–321.
[14] L. Maldonado, M.O. Hoque, Epigenomics and ovarian carcinoma, Biomark Med 4 (4) (2010) 543–570.
[15] B.S. Gloss, G. Samimi, Epigenetic biomarkers in epithelial ovarian cancer, Cancer Lett 342 (2) (2014) 257–263.
[16] C. Nero, F. Ciccarone, A. Pietragalla, G. Scambia, PTEN and gynecological cancers, Cancers (Basel) 11 (10) (2019).
[17] K. Lohmussaar, O. Kopper, J. Korving, H. Begthel, C.P.H. Vreuls, J.H. van Es, H. Clevers, Assessing the origin of high-grade serous ovarian cancer using CRISPR–modification of mouse organoids, Nat Commun 11 (1) (2020) 2660.
[18] B.L. Theriault, H.D. Basavarajappa, H. Lim, S. Pajovic, B.L. Gallie, T.W. Corson, Transcriptional and epigenetic regulation of KIF14 overexpression in ovarian cancer, PLoS One 9 (3) (2014) e91540.
[19] M.T. Gyparaki, A.G. Papavassiliou, Epigenetic pathways offertargets for ovarian cancer treatment, Clin Breast Cancer 18 (3) (2018) 189–191.
[20] D. Pils, P. Horak, P. Vanhara, M. Anees, M. Petz, A. Alfanz, A. Gugerell, M. Wittinger, A. Gleiss, V. Auner, D. Tong, R. Zeillinger, E.I. Braicu, J. Sehouli, M. Krainer, Methylation status of TUSC3 is a prognostic factor in ovarian cancer, Cancer 119 (5) (2013) 946–954.
[21] J. Kwong, J.Y. Lee, K.K. Wong, X. Zhou, D.T. Wong, K.W. Lo, W.R. Welch, R.S. Berkowitz, S.C. Mok, Candidate tumor-suppressor gene DLEC1 is frequently downregulated by promoter hypermethylation and histone hypoacetylation in human epithelial ovarian cancer, Neoplasia 8 (4) (2006) 268–278.
[22] W.W. Li, O.R. Johnson-Ajinwo, F.I. Uche, Advances of plant-derived natural products in ovarian cancer therapy, International Journal of Cancer Research and Prevention 9 (1) (2016) 81–105.
[23] A. Erdmann, L. Halby, J. Fahy, P.B. Arimondo, Targeting DNA methylation with small molecules: what's next? J Med Chem 58 (6) (2015) 2569–2583.
[24] M.B. Pappalardi, K. Keenan, M. Cockerill, W.A. Kellner, A. Stowell, C. Sherk, K. Wong, S. Pathuri, J. Briand, M. Steidel, P. Chapman, A. Groy, A.K. Wiseman, C.F. McHugh, N. Campobasso, A.P. Graves, E. Fairweather, T. Werner, A. Raoof, R.J. Butlin, L. Rueda, J.R. Horton, D.T. Fosbenner, C. Zhang, J.L. Handler, M. Muliaditan, M. Mebrahtu, J.P. Jaworski, D.E. McNulty, C. Burt, H.C. Eberl, A.N. Taylor, T. Ho, S. Merrihew, S.W. Foley, A. Rutkowska, M. Li, S.P. Romeril, K. Goldberg, X. Zhang, C.S. Kershaw, M. Bantscheff, A.J. Jurewicz, E. Minthorn, P. Grandi, M. Patel, A.B. Benowitz, H.P. Mohammad, A.G. Gilmartin, R.K. Prinjha, D. Ogilvie, C. Carpenter, D. Heerding, S.B. Baylin, P.A. Jones, X. Cheng, B.W. King, J.I. Luengo, A.M. Jordan, I. Waddell, R.G. Kruger, M.T. McCabe, Discovery of a first-in-class reversible DNMT1-selective inhibitor with improved tolerability and efficacy in acute myeloid leukemia, Nat Cancer 2 (10) (2021) 1002–1017.
[25] K. Jasek, P. Kubatka, M. Samec, A. Liskova, K. Smejkal, D. Vybohova, O. Bugos, K. Biskupska-Bodova, T. Bielik, P. Zubor, J. Danko, M. Adamkov, T.K. Kwon, D. Busselberg, DNA methylation status in cancer disease: modulations by plant-derived natural compounds and dietary interventions, Biomolecules 9 (7) (2019).
[26] Y. Xu, D. Su, L. Zhu, S. Zhang, S. Ma, K. Wu, Q. Yuan, N. Lin, S-allylcysteine suppresses ovarian cancer cell proliferation by DNA methylation through DNMT1, J Ovarian Res 11 (1) (2018) 39.
[27] L. Zhao, H. Shou, L. Chen, W. Gao, C. Fang, P. Zhang, Effects of ginsenoside Rg3 on epigenetic modification in ovarian cancer cells, Oncol Rep 41 (6) (2019) 3209–3218.

[28] Y. Xiang, Z. Guo, P. Zhu, J. Chen, Y. Huang, Traditional Chinese medicine as a cancer treatment: Modern perspectives of ancient but advanced science, Cancer Med 8 (5) (2019) 1958–1975.
[29] K.H. Lee, E.S. Huang, C. Piantadosi, J.S. Pagano, T.A. Geissman, Cytotoxicity of sesquiterpene lactones, Cancer Res 31 (11) (1971) 1649–1654.
[30] A. Coricello, J.D. Adams, E.J. Lien, C. Nguyen, F. Perri, T.J. Williams, F. Aiello, A walk in nature: sesquiterpene lactones as multi-target agents involved in inflammatory pathways, Curr Med Chem 27 (9) (2020) 1501–1514.
[31] G. Babaei, A. Aliarab, S. Abroon, Y. Rasmi, S.G. Aziz, Application of sesquiterpene lactone: A new promising way for cancer therapy based on anticancer activity, Biomed Pharmacother 106 (2018) 239–246.
[32] A. Ghantous, H. Gali-Muhtasib, H. Vuorela, N.A. Saliba, N. Darwiche, What made sesquiterpene lactones reach cancer clinical trials? Drug Discov Today 15 (15-16) (2010) 668–678.
[33] Y. Ren, J. Yu, A.D. Kinghorn, Development of Anticancer Agents from Plant-Derived Sesquiterpene Lactones, Curr Med Chem 23 (23) (2016) 2397–2420.
[34] Y. Zheng, C.Q. Ke, S. Zhou, L. Feng, C. Tang, Y. Ye, Cytotoxic guaianolides and seco-guaianolides from Artemisia atrovirens, Fitoterapia 151 (2021) 104900.
[35] T. Guardia, A.O. Juarez, E. Guerreiro, J.A. Guzman, L. Pelzer, Anti-inflammatory activity and effect on gastric acid secretion of dehydroleucodine isolated from Artemisia douglasiana, J Ethnopharmacol 88 (2-3) (2003) 195–198.
[36] A.B. Penissi, T.H. Fogal, J.A. Guzman, R.S. Piezzi, Gastroduodenal mucosal protection induced by dehydroleucodine - Mucus secretion and role of monoamines, Digest Dis Sci 43 (4) (1998) 791–798.
[37] A.B. Penissi, M.E. Vera, M.L. Mariani, M.I. Rudolph, J.P. Cenal, J.C. de Rosas, T.H. Fogal, C.E. Tonn, L.S. Favier, O.S. Giordano, R.S. Piezzi, Novel anti-ulcer alpha,beta-unsaturated lactones inhibit compound 48/80-induced mast cell degranulation, Eur J Pharmacol 612 (1-3) (2009) 122–130.
[38] R.C. Coll, P.M. Vargas, M.L. Mariani, A.B. Penissi, Natural alpha,beta-unsaturated lactones inhibit neuropeptide-induced mast cell activation in an in vitro model of neurogenic inflammation, Inflamm Res 69 (10) (2020) 1039–1051.
[39] V.V. Costantino, L. Lobos-Gonzalez, J. Ibanez, D. Fernandez, F.D. Cuello-Carrion, M.A. Valenzuela, M.A. Barbieri, S.N. Semino, G.A. Jahn, A.F. Quest, L.A. Lopez, Dehydroleucodine inhibits tumor growth in a preclinical melanoma model by inducing cell cycle arrest, senescence and apoptosis, Cancer Lett 372 (1) (2016) 10–23.
[40] N. Bailon-Moscoso, G. Gonzalez-Arevalo, G. Velasquez-Rojas, O. Malagon, G. Vidari, A. Zentella-Dehesa, E.A. Ratovitski, P. Ostrosky-Wegman, Phytometabolite dehydroleucodine induces cell cycle arrest, apoptosis, and DNA damage in human astrocytoma cells through p73/p53 regulation, PLoS One 10 (8) (2015) e0136527.
[41] P.E. Ordonez, K.K. Sharma, L.M. Bystrom, M.A. Alas, R.G. Enriquez, O. Malagon, D.E. Jones, M.L. Guzman, C.M. Compadre, Dehydroleucodine, a sesquiterpene lactone from Gynoxys verrucosa, demonstrates cytotoxic activity against human leukemia cells, J Nat Prod 79 (4) (2016) 691–696.
[42] Y. Cai, K.W. Gao, B. Peng, Z.J. Xu, J.W. Peng, J.N. Li, X. Chen, S.S. Zeng, K. Hu, Y.L. Yan, Alantolactone: a natural plant extract as a potential therapeutic agent for cancer, Front Pharmacol 12 (2021).
[43] P. Zhao, Z. Pan, Y. Luo, L. Zhang, X. Li, G. Zhang, Y. Zhang, R. Cui, M. Sun, X. Zhang, Alantolactone induces apoptosis and cell cycle arrest on lung squamous cancer SK-MES-1 Cells, J Biochem Mol Toxicol 29 (5) (2015) 199–206.
[44] J. Liu, Z. Yang, Y. Kong, Y. He, Y. Xu, X. Cao, Antitumor activity of alantolactone in lung cancer cell lines NCI-H1299 and Anip973, J Food Biochem 43 (9) (2019) e12972.
[45] X. Wang, Z. Yu, C. Wang, W. Cheng, X. Tian, X. Huo, Y. Wang, C. Sun, L. Feng, J. Xing, Y. Lan, D. Sun, Q. Hou, B. Zhang, X. Ma, B. Zhang, Alantolactone, a natural sesquiterpene lactone, has potent antitumor activity against glioblastoma by targeting IKKbeta kinase activity and interrupting NF-kappaB/COX-2-mediated signaling cascades, J Exp Clin Cancer Res 36 (1) (2017) 93.
[46] C. Yin, X. Dai, X. Huang, W. Zhu, X. Chen, Q. Zhou, C. Wang, C. Zhao, P. Zou, G. Liang, V. Rajamanickam, O. Wang, X. Zhang, R. Cui, Alantolactone promotes ER stress-mediated apoptosis by inhibition of TrxR1 in triple-negative breast cancer cell lines and in a mouse model, J Cell Mol Med 23 (3) (2019) 2194–2206.
[47] L.L. Yuan, Z. Wang, D.Y. Zhang, J.H. Wang, Metabonomic study of the intervention effects of Parthenolide on anti-thyroid cancer activity, J Chromatogr B 1150 (2020).
[48] J.Z. Zhang, X. Hu, W.Y. Gao, Z. Qu, H.M. Guo, Z. Liu, C.X. Liu, Pharmacokinetic study on costunolide and dehydrocostuslactone after oral administration of traditional medicine Aucklandia lappa Decne. by LC/MS/MS, J Ethnopharmacol 151 (1) (2014) 191–197.
[49] S. Okubo, T. Ohta, H. Fujita, Y. Shoyama, T. Uto, Costunolide and dehydrocostuslactone from Saussurea lappa root inhibit autophagy in hepatocellular carcinoma cells, J Nat Med 75 (1) (2021) 240–245.
[50] Z. Liu, S. Liu, Z. Xie, R.E. Pavlovicz, J. Wu, P. Chen, J. Aimiuwu, J. Pang, D. Bhasin, P. Neviani, J.R. Fuchs, C. Plass, P.K. Li, C. Li, T.H. Huang, L.C. Wu, L. Rush, H. Wang, D. Perrotti, G. Marcucci, K.K. Chan, Modulation of DNA methylation by a sesquiterpene lactone parthenolide, J Pharmacol Exp Ther 329 (2) (2009) 505–514.
[51] I.E. Fadayomi, N. Forsyth, W.W. Li, Role of sesquiterpene lactones against human ovarian cancer, Biochemical Pharmacology 139 (SI) (2017) 134–135.
[52] J.L. Banks, H.S. Beard, Y. Cao, A.E. Cho, W. Damm, R. Farid, A.K. Felts, T.A. Halgren, D.T. Mainz, J.R. Maple, R. Murphy, D.M. Philipp, M.P. Repasky, L.Y. Zhang, B.J. Berne, R.A. Friesner, E. Gallicchio, R.M. Levy, Integrated Modeling Program, Applied Chemical Theory (IMPACT), J Comput Chem 26 (16) (2005) 1752–1780.
[53] Z.M. Zhang, R. Lu, P. Wang, Y. Yu, D. Chen, L. Gao, S. Liu, D. Ji, S.B. Rothbart, Y. Wang, G.G. Wang, J. Song, Structural basis for DNMT3A-mediated de novo DNA methylation, Nature 554 (7692) (2018) 387–391.
[54] N. Eswar, B. Webb, M.A. Marti-Renom, M.S. Madhusudhan, D. Eramian, M.Y. Shen, U. Pieper, A. Sali, Comparative protein structure modeling using Modeller, Curr Protoc Bioinformatics Chapter 5 (2006) Unit-5 6.
[55] H.M. Berman, J. Westbrook, Z. Feng, G. Gilliland, T.N. Bhat, H. Weissig, I.N. Shindyalov, P.E. Bourne, The Protein Data Bank, Nucleic Acids Res 28 (1) (2000) 235–242.
[56] G.M. Sastry, M. Adzhigirey, T. Day, R. Annabhimoju, W. Sherman, Protein and ligand preparation: parameters, protocols, and influence on virtual screening enrichments, J Comput Aided Mol Des 27 (3) (2013) 221–234.
[57] R.A. Laskowski, M.W. MacArthur, D.S. Moss, J.M. Thornton, PROCHECK: a program to check the stereochemical quality of protein structures, Journal of Applied Crystallography 26 (2) (1993) 283–291.
[58] R.A. Friesner, J.L. Banks, R.B. Murphy, T.A. Halgren, J.J. Klicic, D.T. Mainz, M.P. Repasky, E.H. Knoll, M. Shelley, J.K. Perry, D.E. Shaw, P. Francis, P.S. Shenkin, Glide: a new approach for rapid, accurate docking and scoring. 1. Method and assessment of docking accuracy, J Med Chem 47 (7) (2004) 1739–1749.
[59] R.A. Friesner, R.B. Murphy, M.P. Repasky, L.L. Frye, J.R. Greenwood, T.A. Halgren, P.C. Sanschagrin, D.T. Mainz, Extra precision glide: docking and scoring incorporating a model of hydrophobic enclosure for protein-ligand complexes, J Med Chem 49 (21) (2006) 6177–6196.
[60] T.A. Halgren, R.B. Murphy, R.A. Friesner, H.S. Beard, L.L. Frye, W.T. Pollard, J.L. Banks, Glide: a new approach for rapid, accurate docking and scoring. 2. Enrichment factors in database screening, J Med Chem 47 (7) (2004) 1750–1759.
[61] G.M. Morris, R. Huey, W. Lindstrom, M.F. Sanner, R.K. Belew, D.S. Goodsell, A.J. Olson, AutoDock4 and AutoDockTools4: Automated docking with selective receptor flexibility, J Comput Chem 30 (16) (2009) 2785–2791.
[62] O. Trott, A.J. Olson, AutoDock Vina: improving the speed and accuracy of docking with a new scoring function, efficient optimization, and multithreading, J Comput Chem 31 (2) (2010) 455–461.
[63] O.R. Johnson-Ajinwo, A. Richardson, W.W. Li, Cytotoxic effects of stem bark extracts and pure compounds from Margaritaria discoidea on human ovarian cancer cell lines, Phytomedicine 22 (1) (2015) 1–4.
[64] F.I. Uche, F.P. Drijfhout, J. McCullagh, A. Richardson, W.W. Li, Cytotoxicity effects and apoptosis induction by bisbenzylisoquinoline alkaloids from Triclisia subcordata, Phytother Res 30 (9) (2016) 1533–1539.
[65] I.E. Fadayomi, O.R. Johnson-Ajinwo, E. Pires, J. McCullagh, T.D.W. Claridge, N.R. Forsyth, W.W. Li, Clerodane diterpenoids from an edible plant Justicia insularis: discovery, cytotoxicity, and apoptosis induction in human ovarian cancer cells, Molecules 26 (19) (2021).
[66] K.J. Livak, T.D. Schmittgen, Analysis of relative gene expression data using real–time quantitative PCR and the 2(-Delta Delta C(T)) Method, Methods 25 (4) (2001) 402–408.
[67] C. Eurtivong, J. Reynisson, The Development of a Weighted Index to Optimise Compound Libraries for High Throughput Screening, Mol Inform 38 (3) (2019) e1800068.
[68] C.A. Lipinski, F. Lombardo, B.W. Dominy, P.J. Feeney, Experimental and computational approaches to estimate solubility and permeability in drug discovery and development settings, Adv Drug Deliv Rev 46 (1-3) (2001) 3–26.
[69] A. Sali, T.L. Blundell, Comparative protein modelling by satisfaction of spatial restraints, J Mol Biol 234 (3) (1993) 779–815.
[70] M.K. Yadav, S.W. Park, S.W. Chae, J.J. Song, Sinefungin, a natural nucleoside analogue of S-adenosylmethionine, inhibits Streptococcus pneumoniae biofilm growth, Biomed Res Int 2014 (2014) 156987.
[71] M.J. Yebra, J. Sanchez, C.G. Martin, C. Hardisson, C. Barbes, The effect of sinefungin and synthetic analogues on RNA and DNA methyltransferases from Streptomyces, J Antibiot (Tokyo) 44 (10) (1991) 1141–1147.
[72] C. Stresemann, B. Brueckner, T. Musch, H. Stopper, F. Lyko, Functional diversity of DNA methyltransferase inhibitors in human cancer cell lines, Cancer Res 66 (5) (2006) 2794–2800.
[73] C. Stresemann, F. Lyko, Modes of action of the DNA methyltransferase inhibitors azacytidine and decitabine, Int J Cancer 123 (1) (2008) 8–13.
[74] R. Hino, H. Uozaki, N. Murakami, T. Ushiku, A. Shinozaki, S. Ishikawa, T. Morikawa, T. Nakaya, T. Sakatani, K. Takada, M. Fukayama, Activation of DNA methyltransferase 1 by EBV latent membrane protein 2A leads to promoter hypermethylation of PTEN gene in gastric carcinoma, Cancer Res 69 (7) (2009) 2766–2774.
[75] V.V. Costantino, S.F. Mansilla, J. Speroni, C. Amaya, D. Cuello-Carrion, D.R. Ciocca, H.A. Priestap, M.A. Barbieri, V. Gottifredi, L.A. Lopez, The sesquiterpene lactone dehydroleucodine triggers senescence and apoptosis in association with accumulation of DNA damage markers, PLoS One 8 (1) (2013) e53168.
[76] A. Ahluwalia, J.A. Hurteau, R.M. Bigsby, K.P. Nephew, DNA methylation in ovarian cancer. II. Expression of DNA methyltransferases in ovarian cancer cell lines and normal ovarian epithelial cells, Gynecol Oncol 82 (2) (2001) 299–304.
[77] X. Kang, H. Wang, Y. Li, Y. Xiao, L. Zhao, T. Zhang, S. Zhou, X. Zhou, Y. Li, Z. Shou, C. Chen, B. Li, Alantolactone induces apoptosis through ROS-mediated AKT pathway and inhibition of PINK1-mediated mitophagy in human HepG2 cells, Artif Cells Nanomed Biotechnol 47 (1) (2019) 1961–1970.